

Search for the pair production of scalar top quarks in the acoplanar charm jet final state in $p\bar{p}$ collisions at $\sqrt{s} = 1.96$ TeV

V.M. Abazov,³⁵ B. Abbott,⁷⁵ M. Abolins,⁶⁵ B.S. Acharya,²⁸ M. Adams,⁵¹ T. Adams,⁴⁹ E. Aguilo,⁵ S.H. Ahn,³⁰ M. Ahsan,⁵⁹ G.D. Alexeev,³⁵ G. Alkhazov,³⁹ A. Alton,⁶⁴ G. Alverson,⁶³ G.A. Alves,² M. Anastasoiaie,³⁴ L.S. Ancu,³⁴ T. Andeen,⁵³ S. Anderson,⁴⁵ B. Andrieu,¹⁶ M.S. Anzelc,⁵³ Y. Arnoud,¹³ M. Arov,⁵² A. Askew,⁴⁹ B. Åsman,⁴⁰ A.C.S. Assis Jesus,³ O. Atramentov,⁴⁹ C. Autermann,²⁰ C. Avila,⁷ C. Ay,²³ F. Badaud,¹² A. Baden,⁶¹ L. Bagby,⁵² B. Baldin,⁵⁰ D.V. Bandurin,⁵⁹ P. Banerjee,²⁸ S. Banerjee,²⁸ E. Barberis,⁶³ P. Bargassa,⁸⁰ P. Baringer,⁵⁸ C. Barnes,⁴³ J. Barreto,² J.F. Bartlett,⁵⁰ U. Bassler,¹⁶ D. Bauer,⁴³ S. Beale,⁵ A. Bean,⁵⁸ M. Begalli,³ M. Begel,⁷¹ C. Belanger-Champagne,⁴⁰ L. Bellantoni,⁵⁰ A. Bellavance,⁶⁷ J.A. Benitez,⁶⁵ S.B. Beri,²⁶ G. Bernardi,¹⁶ R. Bernhard,⁴¹ L. Berntzon,¹⁴ I. Bertram,⁴² M. Besançon,¹⁷ R. Beuselinck,⁴³ V.A. Bezzubov,³⁸ P.C. Bhat,⁵⁰ V. Bhatnagar,²⁶ M. Binder,²⁴ C. Biscarat,¹⁹ I. Blackler,⁴³ G. Blazey,⁵² F. Blekman,⁴³ S. Blessing,⁴⁹ D. Bloch,¹⁸ K. Bloom,⁶⁷ U. Blumenschein,²² A. Boehnlein,⁵⁰ T.A. Bolton,⁵⁹ G. Borissov,⁴² K. Bos,³³ T. Bose,⁷⁷ A. Brandt,⁷⁸ R. Brock,⁶⁵ G. Brooijmans,⁷⁰ A. Bross,⁵⁰ D. Brown,⁷⁸ N.J. Buchanan,⁴⁹ D. Buchholz,⁵³ M. Buehler,⁹¹ V. Buescher,²² S. Burdin,⁵⁰ S. Burke,⁴⁵ T.H. Burnett,⁸² E. Busato,¹⁶ C.P. Buszello,⁴³ J.M. Butler,⁶² P. Calfayan,²⁴ S. Calvet,¹⁴ J. Cammin,⁷¹ S. Caron,³³ W. Carvalho,³ B.C.K. Casey,⁷⁷ N.M. Cason,⁵⁵ H. Castilla-Valdez,³² S. Chakrabarti,¹⁷ D. Chakraborty,⁵² K.M. Chan,⁷¹ A. Chandra,⁴⁸ F. Charles,¹⁸ E. Cheu,⁴⁵ F. Chevallier,¹³ D.K. Cho,⁶² S. Choi,³¹ B. Choudhary,²⁷ L. Christofek,⁷⁷ D. Claes,⁶⁷ B. Clément,¹⁸ C. Clément,⁴⁰ Y. Coadou,⁵ M. Cooke,⁸⁰ W.E. Cooper,⁵⁰ D. Coppage,⁵⁸ M. Corcoran,⁸⁰ F. Couderc,¹⁷ M.-C. Cousinou,¹⁴ B. Cox,⁴⁴ S. Crépe-Renaudin,¹³ D. Cutts,⁷⁷ M. Cwiok,²⁹ H. da Motta,² A. Das,⁶² M. Das,⁶⁰ B. Davies,⁴² G. Davies,⁴³ K. De,⁷⁸ P. de Jong,³³ S.J. de Jong,³⁴ E. De La Cruz-Burelo,⁶⁴ C. De Oliveira Martins,³ J.D. Degenhardt,⁶⁴ F. Déliot,¹⁷ M. Demarteau,⁵⁰ R. Demina,⁷¹ D. Denisov,⁵⁰ S.P. Denisov,³⁸ S. Desai,⁵⁰ H.T. Diehl,⁵⁰ M. Diesburg,⁵⁰ M. Doidge,⁴² A. Dominguez,⁶⁷ H. Dong,⁷² L.V. Dudko,³⁷ L. Duflot,¹⁵ S.R. Dugad,²⁸ D. Duggan,⁴⁹ A. Duperrin,¹⁴ J. Dyer,⁶⁵ A. Dyshkant,⁵² M. Eads,⁶⁷ D. Edmunds,⁶⁵ J. Ellison,⁴⁸ J. Elmsheuser,²⁴ V.D. Elvira,⁵⁰ Y. Enari,⁷⁷ S. Eno,⁶¹ P. Ermolov,³⁷ H. Evans,⁵⁴ A. Evdokimov,³⁶ V.N. Evdokimov,³⁸ L. Felgioni,⁶² A.V. Ferapontov,⁵⁹ T. Ferbel,⁷¹ F. Fiedler,²⁴ F. Filthaut,³⁴ W. Fisher,⁵⁰ H.E. Fisk,⁵⁰ I. Fleck,²² M. Ford,⁴⁴ M. Fortner,⁵² H. Fox,²² S. Fu,⁵⁰ S. Fuess,⁵⁰ T. Gadfort,⁸² C.F. Galea,³⁴ E. Gallas,⁵⁰ E. Galyaev,⁵⁵ C. Garcia,⁷¹ A. Garcia-Bellido,⁸² J. Gardner,⁵⁸ V. Gavrilov,³⁶ A. Gay,¹⁸ P. Gay,¹² W. Geist,¹⁸ D. Gelé,¹⁸ R. Gelhaus,⁴⁸ C.E. Gerber,⁵¹ Y. Gershtein,⁴⁹ D. Gillberg,⁵ G. Ginter,⁷¹ N. Gollub,⁴⁰ B. Gómez,⁷ A. Goussiou,⁵⁵ P.D. Grannis,⁷² H. Greenlee,⁵⁰ Z.D. Greenwood,⁶⁰ E.M. Gregores,⁴ G. Grenier,¹⁹ Ph. Gris,¹² J.-F. Grivaz,¹⁵ A. Grohsjean,²⁴ S. Grünendahl,⁵⁰ M.W. Grünwald,²⁹ F. Guo,⁷² J. Guo,⁷² G. Gutierrez,⁵⁰ P. Gutierrez,⁷⁵ A. Haas,⁷⁰ N.J. Hadley,⁶¹ P. Haefner,²⁴ S. Hagopian,⁴⁹ J. Haley,⁶⁸ I. Hall,⁷⁵ R.E. Hall,⁴⁷ L. Han,⁶ K. Hanagaki,⁵⁰ P. Hansson,⁴⁰ K. Harder,⁵⁹ A. Harel,⁷¹ R. Harrington,⁶³ J.M. Hauptman,⁵⁷ R. Hauser,⁶⁵ J. Hays,⁴³ T. Hebbeker,²⁰ D. Hedin,⁵² J.G. Hegeman,³³ J.M. Heinmiller,⁵¹ A.P. Heinson,⁴⁸ U. Heintz,⁶² C. Hensel,⁵⁸ K. Herner,⁷² G. Hesketh,⁶³ M.D. Hildreth,⁵⁵ R. Hirosky,⁸¹ J.D. Hobbs,⁷² B. Hoeneisen,¹¹ H. Hoeth,²⁵ M. Hohlfeld,¹⁵ S.J. Hong,³⁰ R. Hooper,⁷⁷ P. Houben,³³ Y. Hu,⁷² Z. Hubacek,⁹ V. Hynek,⁸ I. Iashvili,⁶⁹ R. Illingworth,⁵⁰ A.S. Ito,⁵⁰ S. Jabeen,⁶² M. Jaffré,¹⁵ S. Jain,⁷⁵ K. Jakobs,²² C. Jarvis,⁶¹ A. Jenkins,⁴³ R. Jesik,⁴³ K. Johns,⁴⁵ C. Johnson,⁷⁰ M. Johnson,⁵⁰ A. Jonckheere,⁵⁰ P. Jonsson,⁴³ A. Juste,⁵⁰ D. Käfer,²⁰ S. Kahn,⁷³ E. Kajfasz,¹⁴ A.M. Kalinin,³⁵ J.M. Kalk,⁶⁰ J.R. Kalk,⁶⁵ S. Kappler,²⁰ D. Karmanov,³⁷ J. Kasper,⁶² P. Kasper,⁵⁰ I. Katsanos,⁷⁰ D. Kau,⁴⁹ R. Kaur,²⁶ R. Kehoe,⁷⁹ S. Kermiche,¹⁴ N. Khalatyan,⁶² A. Khanov,⁷⁶ A. Kharchilava,⁶⁹ Y.M. Kharzheev,³⁵ D. Khatidze,⁷⁰ H. Kim,⁷⁸ T.J. Kim,³⁰ M.H. Kirby,³⁴ B. Klima,⁵⁰ J.M. Kohli,²⁶ J.-P. Konrath,²² M. Kopal,⁷⁵ V.M. Korablev,³⁸ J. Kotcher,⁷³ B. Kothari,⁷⁰ A. Koubarovsky,³⁷ A.V. Kozelov,³⁸ D. Krop,⁵⁴ A. Kryemadhi,⁸¹ T. Kuhl,²³ A. Kumar,⁶⁹ S. Kunori,⁶¹ A. Kupco,¹⁰ T. Kurča,¹⁹ J. Kvita,⁸ D. Lam,⁵⁵ S. Lammers,⁷⁰ G. Landsberg,⁷⁷ J. Lazoflores,⁴⁹ A.-C. Le Bihan,¹⁸ P. Lebrun,¹⁹ W.M. Lee,⁵² A. Leflat,³⁷ F. Lehner,⁴¹ V. Lesne,¹² J. Leveque,⁴⁵ P. Lewis,⁴³ J. Li,⁷⁸ L. Li,⁴⁸ Q.Z. Li,⁵⁰ J.G.R. Lima,⁵² D. Lincoln,⁵⁰ J. Linnemann,⁶⁵ V.V. Lipaev,³⁸ R. Lipton,⁵⁰ Z. Liu,⁵ L. Lobo,⁴³ A. Lobodenko,³⁹ M. Lokajicek,¹⁰ A. Lounis,¹⁸ P. Love,⁴² H.J. Lubatti,⁸² M. Lynker,⁵⁵ A.L. Lyon,⁵⁰ A.K.A. Maciel,² R.J. Madaras,⁴⁶ P. Mättig,²⁵ C. Magass,²⁰ A. Magerkurth,⁶⁴ A.-M. Magnan,¹³ N. Makovec,¹⁵ P.K. Mal,⁵⁵ H.B. Malbouissou,³ S. Malik,⁶⁷ V.L. Malyshev,³⁵ H.S. Mao,⁵⁰ Y. Maravin,⁵⁹ M. Martens,⁵⁰ R. McCarthy,⁷² D. Meder,²³ A. Melnitchouk,⁶⁶ A. Mendes,¹⁴ L. Mendoza,⁷ M. Merkin,³⁷ K.W. Merritt,⁵⁰ A. Meyer,²⁰ J. Meyer,²¹ M. Michaut,¹⁷ H. Miettinen,⁸⁰ T. Millet,¹⁹ J. Mitrevski,⁷⁰ J. Molina,³ R.K. Mommsen,⁴⁴ N.K. Mondal,²⁸ J. Monk,⁴⁴ R.W. Moore,⁵ T. Moulik,⁵⁸

G.S. Muanza,¹⁹ M. Mulders,⁵⁰ M. Mulhearn,⁷⁰ O. Mundal,²² L. Mundim,³ E. Nagy,¹⁴ M. Naimuddin,²⁷ M. Narain,⁶² N.A. Naumann,³⁴ H.A. Neal,⁶⁴ J.P. Negret,⁷ P. Neustroev,³⁹ C. Noeding,²² A. Nomerotski,⁵⁰ S.F. Novaes,⁴ T. Nunnemann,²⁴ V. O'Dell,⁵⁰ D.C. O'Neil,⁵ G. Obrant,³⁹ C. Ochando,¹⁵ V. Oguri,³ N. Oliveira,³ D. Onoprienko,⁵⁹ N. Oshima,⁵⁰ J. Osta,⁵⁵ R. Otec,⁹ G.J. Otero y Garzón,⁵¹ M. Owen,⁴⁴ P. Padley,⁸⁰ N. Parashar,⁵⁶ S.-J. Park,⁷¹ S.K. Park,³⁰ J. Parsons,⁷⁰ R. Partridge,⁷⁷ N. Parua,⁷² A. Patwa,⁷³ G. Pawloski,⁸⁰ P.M. Perea,⁴⁸ K. Peters,⁴⁴ P. Pétroff,¹⁵ M. Petteni,⁴³ R. Piegaiia,¹ J. Piper,⁶⁵ M.-A. Pleier,²¹ P.L.M. Podesta-Lerma,³² V.M. Podstavkov,⁵⁰ Y. Pogorelov,⁵⁵ M.-E. Pol,² A. Pompoš,⁷⁵ B.G. Pope,⁶⁵ A.V. Popov,³⁸ C. Potter,⁵ W.L. Prado da Silva,³ H.B. Prosper,⁴⁹ S. Protopopescu,⁷³ J. Qian,⁶⁴ A. Quadt,²¹ B. Quinn,⁶⁶ M.S. Rangel,² K.J. Rani,²⁸ K. Ranjan,²⁷ P.N. Ratoff,⁴² P. Renkel,⁷⁹ S. Reucroft,⁶³ M. Rijssenbeek,⁷² I. Ripp-Baudot,¹⁸ F. Rizatdinova,⁷⁶ S. Robinson,⁴³ R.F. Rodrigues,³ C. Royon,¹⁷ P. Rubinov,⁵⁰ R. Ruchti,⁵⁵ V.I. Rud,³⁷ G. Sajot,¹³ A. Sánchez-Hernández,³² M.P. Sanders,¹⁶ A. Santoro,³ G. Savage,⁵⁰ L. Sawyer,⁶⁰ T. Scanlon,⁴³ D. Schaile,²⁴ R.D. Schamberger,⁷² Y. Scheglov,³⁹ H. Schellman,⁵³ P. Schieferdecker,²⁴ C. Schmitt,²⁵ C. Schwanenberger,⁴⁴ A. Schwartzman,⁶⁸ R. Schwienhorst,⁶⁵ J. Sekaric,⁴⁹ S. Sengupta,⁴⁹ H. Severini,⁷⁵ E. Shabalina,⁵¹ M. Shamim,⁵⁹ V. Shary,¹⁷ A.A. Shchukin,³⁸ R.K. Shivpuri,²⁷ D. Shpakov,⁵⁰ V. Siccadi,¹⁸ R.A. Sidwell,⁵⁹ V. Simak,⁹ V. Sirotenko,⁵⁰ P. Skubic,⁷⁵ P. Slattery,⁷¹ R.P. Smith,⁵⁰ G.R. Snow,⁶⁷ J. Snow,⁷⁴ S. Snyder,⁷³ S. Söldner-Rembold,⁴⁴ X. Song,⁵² L. Sonnenschein,¹⁶ A. Sopczak,⁴² M. Sosebee,⁷⁸ K. Soustruznik,⁸ M. Souza,² B. Spurlock,⁷⁸ J. Stark,¹³ J. Steele,⁶⁰ V. Stolin,³⁶ A. Stone,⁵¹ D.A. Stoyanova,³⁸ J. Strandberg,⁶⁴ S. Strandberg,⁴⁰ M.A. Strang,⁶⁹ M. Strauss,⁷⁵ R. Ströhmer,²⁴ D. Strom,⁵³ M. Strovink,⁴⁶ L. Stutte,⁵⁰ S. Sumowidagdo,⁴⁹ P. Svoisky,⁵⁵ A. Sznajder,³ M. Talby,¹⁴ P. Tamburello,⁴⁵ W. Taylor,⁵ P. Telford,⁴⁴ J. Temple,⁴⁵ B. Tiller,²⁴ M. Titov,²² V.V. Tokmenin,³⁵ M. Tomoto,⁵⁰ T. Toole,⁶¹ I. Torchiani,²² T. Trefzger,²³ S. Trincaz-Duvoid,¹⁶ D. Tsybychev,⁷² B. Tuchming,¹⁷ C. Tully,⁶⁸ P.M. Tuts,⁷⁰ R. Unalan,⁶⁵ L. Uvarov,³⁹ S. Uvarov,³⁹ S. Uzunyan,⁵² B. Vachon,⁵ P.J. van den Berg,³³ B. van Eijk,³⁴ R. Van Kooten,⁵⁴ W.M. van Leeuwen,³³ N. Varelas,⁵¹ E.W. Varnes,⁴⁵ A. Vartapetian,⁷⁸ I.A. Vasilyev,³⁸ M. Vaupel,²⁵ P. Verdier,¹⁹ L.S. Vertogradov,³⁵ M. Verzocchi,⁵⁰ F. Villeneuve-Seguiier,⁴³ P. Vint,⁴³ J.-R. Vlimant,¹⁶ E. Von Toerne,⁵⁹ M. Voutilainen,^{67,†} M. Vreeswijk,³³ H.D. Wahl,⁴⁹ L. Wang,⁶¹ M.H.L.S Wang,⁵⁰ J. Warchol,⁵⁵ G. Watts,⁸² M. Wayne,⁵⁵ G. Weber,²³ M. Weber,⁵⁰ H. Weerts,⁶⁵ N. Wermes,²¹ M. Wetstein,⁶¹ A. White,⁷⁸ D. Wicke,²⁵ G.W. Wilson,⁵⁸ S.J. Wimpenny,⁴⁸ M. Wobisch,⁵⁰ J. Womersley,⁵⁰ D.R. Wood,⁶³ T.R. Wyatt,⁴⁴ Y. Xie,⁷⁷ S. Yacoob,⁵³ R. Yamada,⁵⁰ M. Yan,⁶¹ T. Yasuda,⁵⁰ Y.A. Yatsunenko,³⁵ K. Yip,⁷³ H.D. Yoo,⁷⁷ S.W. Youn,⁵³ C. Yu,¹³ J. Yu,⁷⁸ A. Yurkewicz,⁷² A. Zatserklyaniy,⁵² C. Zeitnitz,²⁵ D. Zhang,⁵⁰ T. Zhao,⁸² B. Zhou,⁶⁴ J. Zhu,⁷² M. Zielinski,⁷¹ D. Zieminska,⁵⁴ A. Zieminski,⁵⁴ V. Zutshi,⁵² and E.G. Zverev³⁷

(DØ Collaboration)

¹ Universidad de Buenos Aires, Buenos Aires, Argentina

² LAFEX, Centro Brasileiro de Pesquisas Físicas, Rio de Janeiro, Brazil

³ Universidade do Estado do Rio de Janeiro, Rio de Janeiro, Brazil

⁴ Instituto de Física Teórica, Universidade Estadual Paulista, São Paulo, Brazil

⁵ University of Alberta, Edmonton, Alberta, Canada, Simon Fraser University, Burnaby, British Columbia, Canada, York University, Toronto, Ontario, Canada, and McGill University, Montreal, Quebec, Canada

⁶ University of Science and Technology of China, Hefei, People's Republic of China

⁷ Universidad de los Andes, Bogotá, Colombia

⁸ Center for Particle Physics, Charles University, Prague, Czech Republic

⁹ Czech Technical University, Prague, Czech Republic

¹⁰ Center for Particle Physics, Institute of Physics, Academy of Sciences of the Czech Republic, Prague, Czech Republic

¹¹ Universidad San Francisco de Quito, Quito, Ecuador

¹² Laboratoire de Physique Corpusculaire, IN2P3-CNRS, Université Blaise Pascal, Clermont-Ferrand, France

¹³ Laboratoire de Physique Subatomique et de Cosmologie, IN2P3-CNRS, Université de Grenoble 1, Grenoble, France

¹⁴ CPPM, IN2P3-CNRS, Université de la Méditerranée, Marseille, France

¹⁵ IN2P3-CNRS, Laboratoire de l'Accélérateur Linéaire, Orsay, France

¹⁶ LPNHE, IN2P3-CNRS, Universités Paris VI and VII, Paris, France

¹⁷ DAPNIA/Service de Physique des Particules, CEA, Saclay, France

¹⁸ IPHC, IN2P3-CNRS, Université Louis Pasteur, Strasbourg, France, and Université de Haute Alsace, Mulhouse, France

¹⁹ Institut de Physique Nucléaire de Lyon, IN2P3-CNRS, Université Claude Bernard, Villeurbanne, France

²⁰ III. Physikalisches Institut A, RWTH Aachen, Aachen, Germany

²¹ Physikalisches Institut, Universität Bonn, Bonn, Germany

²² Physikalisches Institut, Universität Freiburg, Freiburg, Germany

²³ Institut für Physik, Universität Mainz, Mainz, Germany

²⁴ Ludwig-Maximilians-Universität München, München, Germany

²⁵ Fachbereich Physik, University of Wuppertal, Wuppertal, Germany

²⁶ Panjab University, Chandigarh, India

- ²⁷ Delhi University, Delhi, India
- ²⁸ Tata Institute of Fundamental Research, Mumbai, India
- ²⁹ University College Dublin, Dublin, Ireland
- ³⁰ Korea Detector Laboratory, Korea University, Seoul, Korea
- ³¹ SungKyunKwan University, Suwon, Korea
- ³² CINVESTAV, Mexico City, Mexico
- ³³ FOM-Institute NIKHEF and University of Amsterdam/NIKHEF, Amsterdam, The Netherlands
- ³⁴ Radboud University Nijmegen/NIKHEF, Nijmegen, The Netherlands
- ³⁵ Joint Institute for Nuclear Research, Dubna, Russia
- ³⁶ Institute for Theoretical and Experimental Physics, Moscow, Russia
- ³⁷ Moscow State University, Moscow, Russia
- ³⁸ Institute for High Energy Physics, Protvino, Russia
- ³⁹ Petersburg Nuclear Physics Institute, St. Petersburg, Russia
- ⁴⁰ Lund University, Lund, Sweden, Royal Institute of Technology and Stockholm University, Stockholm, Sweden, and Uppsala University, Uppsala, Sweden
- ⁴¹ Physik Institut der Universität Zürich, Zürich, Switzerland
- ⁴² Lancaster University, Lancaster, United Kingdom
- ⁴³ Imperial College, London, United Kingdom
- ⁴⁴ University of Manchester, Manchester, United Kingdom
- ⁴⁵ University of Arizona, Tucson, Arizona 85721, USA
- ⁴⁶ Lawrence Berkeley National Laboratory and University of California, Berkeley, California 94720, USA
- ⁴⁷ California State University, Fresno, California 93740, USA
- ⁴⁸ University of California, Riverside, California 92521, USA
- ⁴⁹ Florida State University, Tallahassee, Florida 32306, USA
- ⁵⁰ Fermi National Accelerator Laboratory, Batavia, Illinois 60510, USA
- ⁵¹ University of Illinois at Chicago, Chicago, Illinois 60607, USA
- ⁵² Northern Illinois University, DeKalb, Illinois 60115, USA
- ⁵³ Northwestern University, Evanston, Illinois 60208, USA
- ⁵⁴ Indiana University, Bloomington, Indiana 47405, USA
- ⁵⁵ University of Notre Dame, Notre Dame, Indiana 46556, USA
- ⁵⁶ Purdue University Calumet, Hammond, Indiana 46323, USA
- ⁵⁷ Iowa State University, Ames, Iowa 50011, USA
- ⁵⁸ University of Kansas, Lawrence, Kansas 66045, USA
- ⁵⁹ Kansas State University, Manhattan, Kansas 66506, USA
- ⁶⁰ Louisiana Tech University, Ruston, Louisiana 71272, USA
- ⁶¹ University of Maryland, College Park, Maryland 20742, USA
- ⁶² Boston University, Boston, Massachusetts 02215, USA
- ⁶³ Northeastern University, Boston, Massachusetts 02115, USA
- ⁶⁴ University of Michigan, Ann Arbor, Michigan 48109, USA
- ⁶⁵ Michigan State University, East Lansing, Michigan 48824, USA
- ⁶⁶ University of Mississippi, University, Mississippi 38677, USA
- ⁶⁷ University of Nebraska, Lincoln, Nebraska 68588, USA
- ⁶⁸ Princeton University, Princeton, New Jersey 08544, USA
- ⁶⁹ State University of New York, Buffalo, New York 14260, USA
- ⁷⁰ Columbia University, New York, New York 10027, USA
- ⁷¹ University of Rochester, Rochester, New York 14627, USA
- ⁷² State University of New York, Stony Brook, New York 11794, USA
- ⁷³ Brookhaven National Laboratory, Upton, New York 11973, USA
- ⁷⁴ Langston University, Langston, Oklahoma 73050, USA
- ⁷⁵ University of Oklahoma, Norman, Oklahoma 73019, USA
- ⁷⁶ Oklahoma State University, Stillwater, Oklahoma 74078, USA
- ⁷⁷ Brown University, Providence, Rhode Island 02912, USA
- ⁷⁸ University of Texas, Arlington, Texas 76019, USA
- ⁷⁹ Southern Methodist University, Dallas, Texas 75275, USA
- ⁸⁰ Rice University, Houston, Texas 77005, USA
- ⁸¹ University of Virginia, Charlottesville, Virginia 22901, USA
- ⁸² University of Washington, Seattle, Washington 98195, USA

(Dated: November 1, 2006)

A search for the pair production of scalar top quarks, \tilde{t} , has been performed in 360 pb^{-1} of data from $p\bar{p}$ collisions at a center-of-mass energy of 1.96 TeV, collected by the D0 detector at the Fermilab Tevatron collider. The \tilde{t} decay mode considered is $\tilde{t} \rightarrow c\tilde{\chi}_1^0$, where $\tilde{\chi}_1^0$ is the lightest supersymmetric particle. The topology analyzed therefore consists of a pair of acoplanar heavy-flavor jets with

missing transverse energy. The data and standard model expectation are in agreement, and a 95% C.L. exclusion domain in the $(m_{\tilde{t}}, m_{\tilde{\chi}_1^0})$ plane has been determined, extending the domain excluded by previous experiments.

PACS numbers: 14.80.Ly, 12.60.Jv

Supersymmetric (SUSY) models [1] predict the existence of new particles, carrying the same quantum numbers as their standard model (SM) partners, but differing by half a unit of spin. For instance, there are two scalar-quark fields associated with the left- and right-handed degrees of freedom of each ordinary quark. The mass eigenstates result from the diagonalization of a mass matrix, with elements determined by the specific SUSY-breaking pattern. A light SUSY partner of the top quark, or stop, is a generic prediction of models in which the scalar quark masses are equal at the grand unification scale. A first reason is that, due to the impact of the large top quark Yukawa coupling in the renormalization group equations, the diagonal elements of the mass matrix are driven to values smaller than those for the other scalar quarks at the electroweak scale [2]. A second reason is that the off-diagonal terms are proportional to the relevant quark mass, and hence are much larger in the case of the top quark. The mass eigenstates are therefore broadly split, with the mass of the lighter stop \tilde{t} thus driven to an even lower value [3]. Finally, a light stop is a necessary ingredient in the context of electroweak baryogenesis [4].

In models with R -parity conservation [5], the lightest SUSY particle (LSP) is stable, and cosmological constraints imply that it should be neutral and colorless [6]. In a large class of SUSY models, the lightest of the neutralinos — the mass eigenstates resulting from the mixing of the SUSY partners of the neutral gauge and Higgs bosons — is the LSP, which furthermore appears as a viable dark matter candidate. In the following, it will be assumed that R -parity is conserved and that the LSP is the lightest neutralino $\tilde{\chi}_1^0$.

The dominant stop decay modes are expected to be $\tilde{t} \rightarrow t\tilde{\chi}_1^0$ and $\tilde{t} \rightarrow b\tilde{\chi}_1^+$, where the chargino $\tilde{\chi}_1^+$ is the lighter of the two mass eigenstates resulting from the mixing of the SUSY partners of the charged gauge and Higgs bosons. However, in the \tilde{t} mass range of interest in this Letter, the $\tilde{t} \rightarrow t\tilde{\chi}_1^0$ decay mode is kinematically forbidden. In the following, the region of SUSY parameter space with $m_{\tilde{t}} < m_b + m_{\tilde{\chi}_1^+}$ and $m_{\tilde{t}} < M_W + m_b + m_{\tilde{\chi}_1^0}$ is considered, and it is assumed that $\tilde{t} \rightarrow c\tilde{\chi}_1^0$, a flavor-changing loop decay [7], is the only relevant decay mode, i.e., that the tree-level four-body decays [8] $\tilde{t} \rightarrow bf\tilde{f}'\tilde{\chi}_1^0$ can be neglected.

In $p\bar{p}$ collisions, stop pair production proceeds via $q\bar{q}$ annihilation and gluon-gluon fusion. The cross section has very little dependence on SUSY parameters other than the stop mass. At the center-of-mass energy of 1.96 TeV available in Run II of the Fermilab Tevatron col-

lider, it ranges from 15 to 2.25 pb for stop masses from 100 to 140 GeV, as calculated at next-to-leading order (NLO) with PROSPINO [9], for equal renormalization and factorization scales $\mu_{rf} = m_{\tilde{t}}$ and using the CTEQ6.1M parton distribution functions (PDFs) [10]. The final state topology resulting from the $\tilde{t} \rightarrow c\tilde{\chi}_1^0$ decay is a pair of acoplanar jets, with large missing transverse energy \cancel{E}_T carried away by the two weakly interacting LSPs. Previous searches in this topology performed at LEP excluded stop masses smaller than ≈ 100 GeV, essentially independent of the stop- $\tilde{\chi}_1^0$ mass difference [11]. Searches in data from the Run I of the Tevatron [12, 13] extended the domain excluded at LEP to larger stop masses, but for $\tilde{\chi}_1^0$ masses not exceeding ≈ 50 GeV. The largest stop mass excluded was 122 GeV, for $m_{\tilde{\chi}_1^0} = 45$ GeV [13]. In this Letter, we report on a similar search, performed in data collected using the D0 detector during Run II of the Tevatron.

The acoplanar jet topology may arise from new physics processes other than stop pair production. Recently, the D0 Collaboration performed a search for pair production of leptoquarks decaying into a quark and a neutrino [14], which leads to the same topology. The analysis reported here is largely based on that leptoquark search. In the following, only a brief summary of the common aspects is given, while the specific features relevant for the stop search are presented in greater detail. The main differences arise from the LSP mass, which leads to smaller jet transverse energies and to a reduced \cancel{E}_T , compared to the case of leptoquark decays which involve nearly massless neutrinos. Another characteristic feature of stop decays is that charm jets are produced, while first-generation leptoquarks decay to light-flavor jets.

A thorough description of the D0 detector can be found in Ref. [15]. The central tracking system consists of a silicon microstrip tracker and a fiber tracker, both located within a 2 T superconducting solenoidal magnet. A liquid-argon and uranium calorimeter covers pseudorapidities $|\eta| \lesssim 4.2$, where $\eta = -\ln[\tan(\theta/2)]$ and θ is the polar angle with respect to the proton beam direction. An outer muon system, covering $|\eta| < 2$, consists of layers of tracking detectors and scintillation counters on both sides of 1.8 T iron toroids.

For this search, ≈ 14 million events collected from April 2003 to August 2004 with a jets + \cancel{E}_T trigger were

analyzed, corresponding to an integrated luminosity¹ of 360 pb^{-1} . The offline analysis utilized jets reconstructed with the iterative midpoint cone algorithm [17] with a cone size of 0.5. Only jets with transverse momentum $p_T > 15 \text{ GeV}$ were considered in the analysis. The \cancel{E}_T was calculated using all calorimeter cells, corrected for the energy calibration of reconstructed jets, as determined from the transverse momentum balance in photon+jet events, and for the momentum of reconstructed muons.

Signal efficiencies and SM backgrounds were evaluated using a full GEANT-3 [18] based simulation of events, with a Poisson average of 0.8 minimum-bias events superimposed, corresponding to the luminosity profile of the data sample analyzed. These simulated events were reconstructed in the same way as the data. In the bulk of events from QCD multijet production, no significant \cancel{E}_T is expected. Jet energy mismeasurements due to the limited detector resolution may however lead to large measured \cancel{E}_T values. This “instrumental background” was not simulated, and its contribution estimated directly from the data. In the following, “standard model (SM) background” stands for “non-QCD standard model (SM) background.” Leptonic W decays, as well as $Z \rightarrow \nu\nu$ are sources of energetic neutrinos, hence of genuine \cancel{E}_T . The SM processes expected to yield the largest background contributions are therefore vector boson production in association with jets. They were generated with ALPGEN 1.3 [19], interfaced with PYTHIA 6.202 [20] for the simulation of initial and final state radiation and for jet hadronization. The PDFs used were CTEQ5L [21]. The NLO cross sections for vector boson production in association with jets were calculated with MCFM 3.4.4 [22]. Vector-boson pair, $t\bar{t}$, and single top quark production were also considered. Signal samples of 10 000 events were generated with PYTHIA and the CTEQ5L PDFs for stop masses ranging from 95 to 145 GeV and for $\tilde{\chi}_1^0$ masses from 40 to 70 GeV, both in steps of 5 GeV.

The following selection criteria were applied, independent of the stop and $\tilde{\chi}_1^0$ masses: there had to be at least two jets; the vector sum $\vec{\cancel{H}}_T$ of all jet transverse momenta ($\vec{\cancel{H}}_T = |\sum_{\text{jets}} \vec{p}_T|$) as well as the missing transverse energy had to exceed 40 GeV; the leading and subleading jets (where jets are ordered according to their transverse momentum) had to be central ($|\eta_{\text{det}}| < 1.5$, where η_{det} is the pseudorapidity measured from the detector center), with transverse momenta exceeding 40 and 20 GeV, respectively, and they had to be confirmed by charged particle tracks [14]; the acoplanarity $\Delta\Phi$ of the two leading jets had to be smaller than 165° , where $\Delta\Phi$ is the difference between the two jet azimuthal angles; the lon-

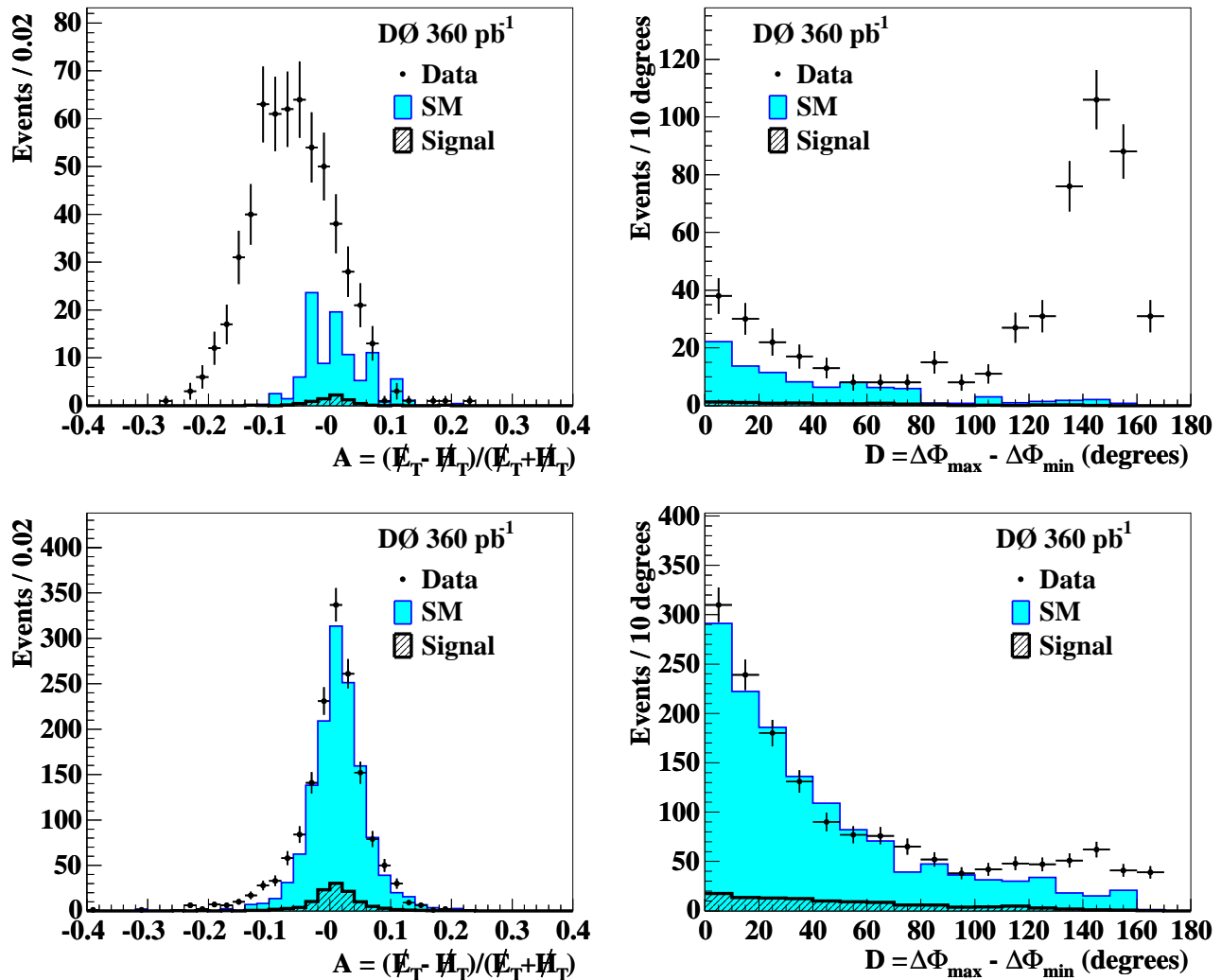
gitudinal position of the primary vertex had to be less than 60 cm away from the center of the detector. At this point, 99 884 events were selected, largely dominated by instrumental background from multijet events. The efficiency for a reference signal with $m_{\tilde{t}} = 140 \text{ GeV}$ and $m_{\tilde{\chi}_1^0} = 60 \text{ GeV}$ was 30%.

The jet multiplicity distribution revealed that most of the selected events contained at least three jets, due to the acoplanarity requirement. Therefore, only events containing exactly two jets were retained, leaving 27 853 data events with an efficiency of 22% for the reference signal. The inefficiency associated with the rejection of events with more than two jets was evaluated, based on studies of jet multiplicities in real and simulated $Z \rightarrow ee$ events with at least two jets, where the two leading jets fulfilled similar selection criteria as in the analysis. This study also showed that the kinematic variables used in the analysis were adequately simulated. Standard model backgrounds from $W \rightarrow \ell\nu + \text{jet}$ processes were greatly reduced by requiring that there be no isolated electron or muon with $p_T > 10 \text{ GeV}$, and no isolated charged particle track with $p_T > 5 \text{ GeV}$ [14]. This retained 22 106 data events, with an efficiency of 19% for the reference signal.

Most of the remaining instrumental background was eliminated by the following requirements. The \cancel{E}_T had to exceed 60 GeV, and the difference $\mathcal{D} = \Delta\Phi_{\text{max}} - \Delta\Phi_{\text{min}}$ had to be smaller than 120° , where $\Delta\Phi_{\text{min}}$ and $\Delta\Phi_{\text{max}}$ are the minimum and maximum of the azimuthal angles between the \cancel{E}_T direction and the directions of the two jets, respectively. These criteria take advantage of the facts that, for the instrumental background, the \cancel{E}_T distribution is steeply decreasing, and its direction tends to be close to that of a mismeasured jet. In addition, the asymmetry $\mathcal{A} = (\cancel{E}_T - \vec{\cancel{H}}_T) / (\cancel{E}_T + \vec{\cancel{H}}_T)$ was required to be larger than -0.05 . This variable is sensitive to the amount of energy deposited in the calorimeter that was not clustered into jets. It can be seen in Fig. 1 that both \mathcal{D} and \mathcal{A} are effective in discriminating SM backgrounds and signal from the instrumental background. After these requirements, 1 348 data events were retained, while $1\,292 \pm 45$ events were expected from SM backgrounds, where the uncertainty is statistical. The efficiency for the reference signal was 13%. There was no evidence at this point for any significant instrumental background remaining. This background has therefore been neglected in the following.

To increase the search sensitivity, advantage was then taken of the presence of charm jets in the signal. A lifetime-based heavy-flavor tagging algorithm was used for this purpose, which involves a probability built from the impact parameter significances of the tracks belonging to a jet [23]. The impact parameter of a track is its distance of closest approach to the event vertex, in a plane perpendicular to the beam axis, and the significance is obtained by normalization to the impact param-

¹ This value differs from the one used in Ref. [14] due to a recent adjustment of the D0 luminosity constant [16].



cc

FIG. 1: Distributions of the asymmetry $\mathcal{A} = (\cancel{E}_T - \cancel{H}_T) / (\cancel{E}_T + \cancel{H}_T)$ with the cut on $\mathcal{D} = \Delta\Phi_{\text{max}} - \Delta\Phi_{\text{min}}$ inverted (top-left) or applied (bottom-left) and of \mathcal{D} with the cut on \mathcal{A} inverted (top-right) or applied (bottom-right) for data (points with error bars), for SM backgrounds (filled histogram), and for a signal with $m_{\tilde{t}} = 140 \text{ GeV}$ and $m_{\tilde{\chi}_1^0} = 60 \text{ GeV}$ (hatched histogram). The \cancel{E}_T cut at 60 GeV has been applied. In the bottom plots, the excesses in data for $\mathcal{A} < -0.05$ and for $\mathcal{D} > 120^\circ$ are attributed to the residual non-simulated instrumental background.

eter uncertainty. This probability is constructed such that its distribution is uniform for light-flavor jets and peaks towards zero for heavy-flavor jets. In order to cope with differences in track reconstruction efficiencies in data and in simulation, the heavy-flavor tagging algorithm was applied directly only to the data, while flavor-dependent tagging probabilities measured in dedicated data samples were applied to the simulated jets. The probability cut used in this analysis was such that typically 4% of the light-flavor jets were tagged (central jets with $p_T \approx 50 \text{ GeV}$). The corresponding typical tagging efficiencies for c and b quark jets were 30% and 65%, respectively. Jets resulting from τ decays were tagged with a typical efficiency of 20%. By requiring that at least one jet be tagged, 183 data events were selected, while

186 ± 16 SM background events were expected, where the uncertainty is statistical. The efficiency for the reference signal was 6.5%.

Since the signal topology depends on the stop and $\tilde{\chi}_1^0$ masses, additional selection criteria on three kinematic variables were simultaneously optimized for each mass combination. These variables were the scalar sum $H_T = \sum_{\text{jets}} |\vec{p}_T|$ of the jet transverse momenta in steps of 20 GeV, \cancel{E}_T in steps of 10 GeV, and $\mathcal{S} = \Delta\Phi_{\text{max}} + \Delta\Phi_{\text{min}}$ in steps of 10° . It can be seen in Fig. 2 that this last variable provides good discrimination between signal and SM backgrounds. For H_T and \cancel{E}_T , the selection retained events above the cut value, while for \mathcal{S} , events below the cut value were selected. For each stop and $\tilde{\chi}_1^0$ mass combination tested, all sets of cuts were considered. For each

set, the value $\langle CL_s \rangle$ of the signal confidence level [24] expected if only background were present was computed, with the systematic uncertainties discussed below taken into account. For a given stop mass, the expected lower limit on $m_{\tilde{\chi}_1^0}$ was determined as the $\tilde{\chi}_1^0$ mass for which $\langle CL_s \rangle = 5\%$, by interpolation across the $m_{\tilde{\chi}_1^0}$ values tested. The set leading to the largest expected lower limit on $m_{\tilde{\chi}_1^0}$ was selected as the optimal one for the stop mass considered. In all cases, a \cancel{E}_T cut at 60 GeV was selected. The results of the optimization for the other variables are given in Table I, together with the numbers of events selected in the data and expected from SM backgrounds. Signal efficiencies and numbers of signal events expected are given in Table II for three mass combinations close to the edge of the sensitivity domain of the analysis.

The distribution of H_T shown in Fig. 2 and the final distribution of \cancel{E}_T shown in Fig. 3 were obtained after optimization for a stop mass of 140 GeV. An excess at large \cancel{E}_T is observed in the data with respect to the expectation: there are eight data events with $\cancel{E}_T > 150$ GeV, while 3.2 ± 1.4 events are expected from SM backgrounds. A detailed scrutiny of those events was performed, that did not reveal any anomaly such as clusterings in some of the kinematic variables, signs of leptons unidentified by the standard algorithms, heavy flavor tagging probabilities different from what is observed in the rest of the selected events. The data taking conditions were also carefully checked for signs of detector malfunctions and visual scans were performed. It can also be noted that such large \cancel{E}_T values are beyond what is expected from a stop signal.

TABLE I: Results of the optimization: stop mass range in GeV, H_T cut value in GeV, and \mathcal{S} cut value in degrees. In all cases, a \cancel{E}_T cut at 60 GeV was selected. The numbers of events observed and expected from SM backgrounds are also given; the first uncertainties are statistical, and the second systematic.

$m_{\tilde{t}}$	H_T	\mathcal{S}	# observed	# expected
95 – 115	> 80	< 260	68	59.9 ± 9.6 $^{+11.7}_{-9.7}$
120	> 80	< 280	89	86.4 ± 11.3 $^{+16.2}_{-14.2}$
125 – 140	> 120	< 280	50	47.0 ± 8.0 $^{+9.7}_{-7.9}$
145	> 120	< 300	57	53.8 ± 8.3 $^{+10.8}_{-9.2}$

The SM background composition is detailed in Table III for the selection optimized for $m_{\tilde{t}} = 140$ GeV. As expected, the largest contributions come from $(Z \rightarrow \nu\nu$ and $W \rightarrow \ell\nu)$ +light-flavor jets. This is due to the loose heavy-flavor tagging criterion which was selected in order to be efficient for charm jets. Vector boson production with heavy-flavor jets gives rather small contributions because of the comparatively small cross sections.

Systematic uncertainties were evaluated for each combination of stop and $\tilde{\chi}_1^0$ masses, according to the cor-

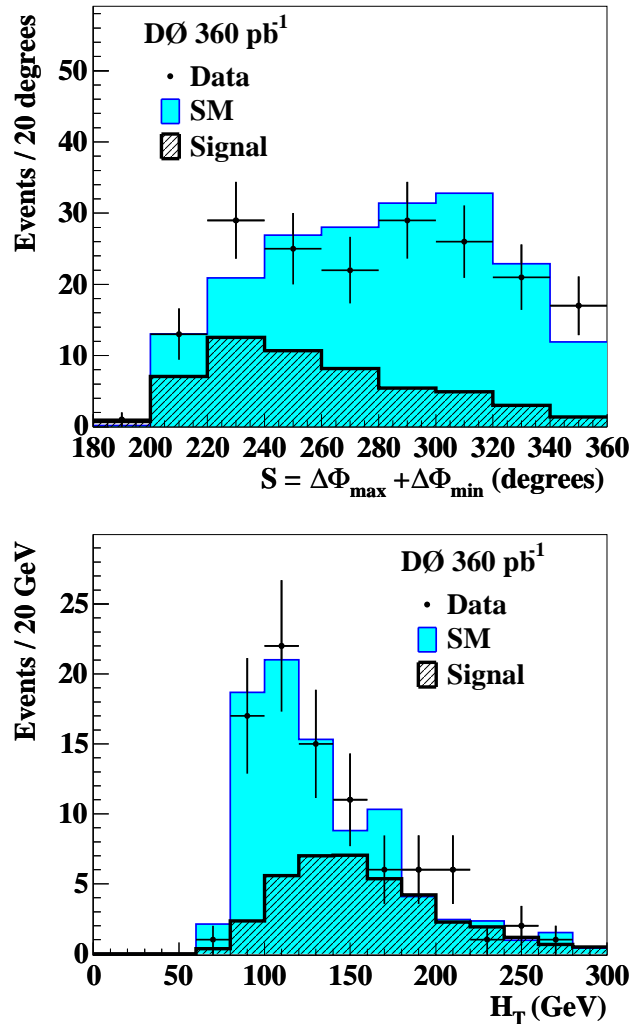


FIG. 2: Distributions of $\mathcal{S} = \Delta\Phi_{\max} + \Delta\Phi_{\min}$ before optimization (top), and of H_T after optimization for $m_{\tilde{t}} = 140$ GeV but with the cut on H_T removed (bottom), for data (points with error bars), for SM backgrounds (filled histogram), and for a signal with $m_{\tilde{t}} = 140$ GeV and $m_{\tilde{\chi}_1^0} = 60$ GeV (hatched histogram).

TABLE II: For three stop and $\tilde{\chi}_1^0$ mass combinations, in GeV, signal efficiencies (Eff.) and numbers of signal events expected, where the first uncertainties are statistical and the second systematic. The stop pair production cross section upper limits at 95% C.L. are also given (σ_{UL}), as well as the NLO theoretical cross section (σ_{Th}), both in pb.

$(m_{\tilde{t}}, m_{\tilde{\chi}_1^0})$	Eff. (%)	# expected	σ_{UL}	σ_{Th}
(100,55)	0.75	40.4 ± 4.6 $^{+5.3}_{-5.4}$	15.8	15.0
(120,65)	2.04	40.0 ± 2.8 $^{+5.6}_{-5.2}$	6.57	5.43
(140,60)	3.74	30.3 ± 1.6 $^{+4.8}_{-5.3}$	2.38	2.25

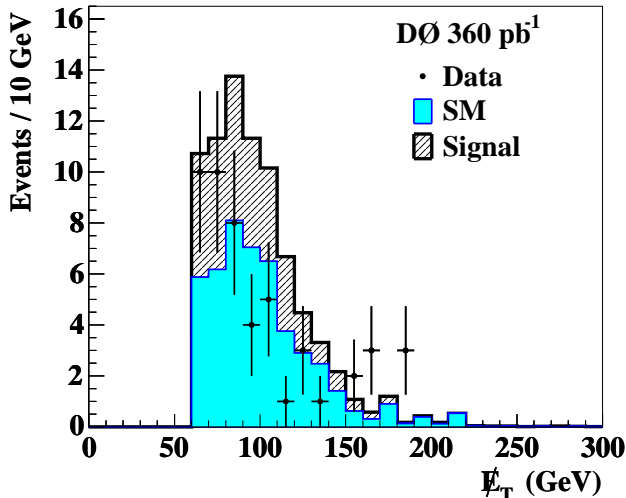


FIG. 3: Final \cancel{E}_T distribution for data (points with error bars), for SM backgrounds (filled histogram), and, on top of the SM backgrounds, for a signal with $m_{\tilde{t}} = 140$ GeV and $m_{\tilde{\chi}_1^0} = 60$ GeV (hatched histogram).

TABLE III: Numbers of events expected from the various SM background processes in the selection optimized for $m_{\tilde{t}} = 140$ GeV. The uncertainties are statistical. In the vector boson + jets backgrounds, “jet” stands for “light-flavor jet.”

SM process	# expected
$Z \rightarrow \nu\nu + \text{jets}$	13.9 ± 2.8
$Z \rightarrow \nu\nu + c\bar{c}$	1.7 ± 0.4
$Z \rightarrow \nu\nu + b\bar{b}$	3.5 ± 0.2
$W \rightarrow \ell\nu + \text{jets}$	19.5 ± 7.4
$W \rightarrow \ell\nu + (c\bar{c} \text{ or } c + \text{jet})$	1.8 ± 0.5
$W \rightarrow \ell\nu + b\bar{b}$	1.5 ± 0.2
$t\bar{t}$ and single top	4.1 ± 0.2
WW, WZ, ZZ	1.1 ± 0.2
Total	47.0 ± 8.0

responding optimized selection criteria. They are listed below for the reference signal. The following are fully correlated between SM-background and signal expectations: from the jet energy calibration and resolution, $^{+13}_{-6}\%$ for the SM background and $^{+3}_{-4}\%$ for the signal; from the jet multiplicity cut, 3%; from the trigger efficiency, 2% after all selection cuts; from the heavy-flavor tagging, 6% for the SM background and 7% for the signal; from the integrated luminosity of the analysis sample, 6%. In addition to the 17% statistical uncertainty of the simulation, the normalization of the SM background expectation carries a 13% uncertainty, as inferred from a comparison of data and simulated ($Z \rightarrow ee$) + 2-jet events. The statistical uncertainty of the signal simulation is 5%. Finally, the uncertainty on the signal efficiency due to the PDF choice was determined to be $^{+6}_{-4}\%$, using the CTEQ6.1M error set [10].

As can be seen in Table I, no significant excess of data was observed in any of the optimized selections. Signal production cross section upper limits were therefore derived with the above systematic uncertainties taken into account. Examples are given in Table II, together with the corresponding theoretical cross sections. To determine an exclusion domain in the $(m_{\tilde{t}}, m_{\tilde{\chi}_1^0})$ plane, the following procedure was used. For a given $m_{\tilde{t}}$ the signal confidence level CL_s was computed as a function of $m_{\tilde{\chi}_1^0}$ in the modified frequentist approach [24], and the 95% C.L. lower limit on $m_{\tilde{\chi}_1^0}$ was determined as the $\tilde{\chi}_1^0$ mass for which $CL_s = 5\%$. In this procedure, the theoretical NLO cross sections predicted by PROSPINO with the CTEQ6.1M PDFs were used. The nominal cross section was obtained for $\mu_{r,f} = m_{\tilde{t}}$. Theoretical uncertainties on the stop pair production cross section arise from the choices of PDFs and of renormalization and factorization scale. The variations observed with the CTEQ6.1M error PDF set, as well as the changes induced when $\mu_{r,f}$ is modified by a factor of two up or down, result in a typically $\pm 20\%$ change in the theoretical cross section when combined in quadrature. The exclusion contour in the $(m_{\tilde{t}}, m_{\tilde{\chi}_1^0})$ plane thus obtained is shown as a solid curve in Fig. 4 for the nominal production cross section. The corresponding expected exclusion contour is shown as a dashed curve. The effect of the PDF and scale uncertainties on the observed exclusion contour is shown as a shaded band.

This analysis, performed under the assumption that the stop decays exclusively into a charm quark and the lightest neutralino, extends the stop and $\tilde{\chi}_1^0$ mass domain excluded by previous experiments [11, 12, 13]. For the nominal stop pair production cross section, the largest stop mass excluded is 141 GeV, obtained for $m_{\tilde{\chi}_1^0} = m_{\tilde{t}} - m_b - m_W = 55$ GeV. Taking into account the theoretical uncertainty on the production cross section, the largest stop mass limit is 134 GeV, obtained for $m_{\tilde{\chi}_1^0} = 48$ GeV.

We thank the staffs at Fermilab and collaborating institutions, and acknowledge support from the DOE and NSF (USA); CEA and CNRS/IN2P3 (France); FASI, Rosatom and RFBR (Russia); CAPES, CNPq, FAPERJ, FAPESP and FUNDUNESP (Brazil); DAE and DST (India); Colciencias (Colombia); CONACyT (Mexico); KRF and KOSEF (Korea); CONICET and UBACyT (Argentina); FOM (The Netherlands); PPARC (United Kingdom); MSMT (Czech Republic); CRC Program, CFI, NSERC and WestGrid Project (Canada); BMBF and DFG (Germany); SFI (Ireland); The Swedish Research Council (Sweden); Research Corporation; Alexander von Humboldt Foundation; and the Marie Curie Program.

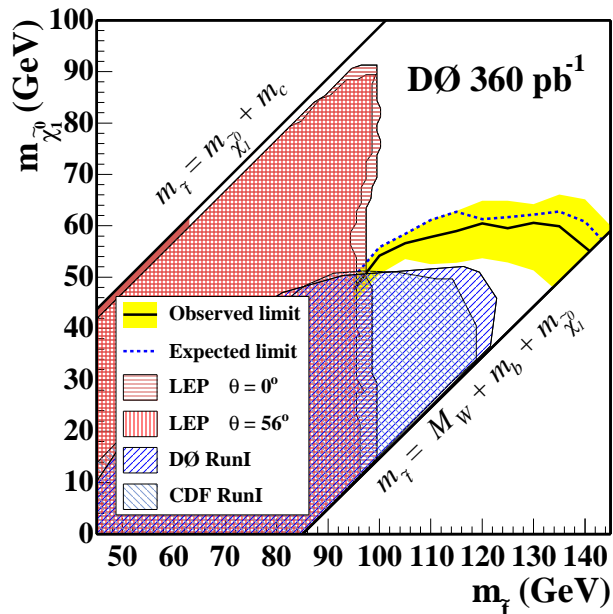


FIG. 4: Domain in the $(m_{\tilde{t}}, m_{\tilde{\chi}_1^0})$ plane excluded at the 95% C.L. by the present search (region below the solid curve), under the assumption that the stop decays exclusively into $c\tilde{\chi}_1^0$ and for the nominal production cross section. The expected exclusion contour is shown as a dashed curve. The effect of increasing or decreasing the production cross section by its uncertainty due to the PDF and μ_{rf} choices is indicated for the observed exclusion contour by the shaded band. Results from previous searches for stop pair production in the $\tilde{t} \rightarrow c\tilde{\chi}_1^0$ decay channel are also indicated [11, 12, 13]. The dark shaded band at small $m_{\tilde{t}} - m_{\tilde{\chi}_1^0}$ is excluded by Ref. [25]. The LEP results are shown for two values of θ , the mixing angle in the stop sector.

[†] Visitor from Helsinki Institute of Physics, Helsinki, Finland.

- [1] H.E. Haber and G.L. Kane, Phys. Rep. **117**, 75 (1985).
 [2] See for instance V. Barger, M.S. Berger and P. Ohmann, Phys. Rev. D **49**, 4908 (1994).

- [3] J. Ellis and S. Rudaz, Phys. Lett. B **128**, 248 (1983).
 [4] M. Quiros, Nucl. Phys. Proc. Suppl. **101**, 401 (2001), and references therein.
 [5] P. Fayet, Phys. Lett. B **69**, 489 (1977).
 [6] J. Ellis *et al.*, Nucl. Phys. B **238**, 453 (1984).
 [7] K.I. Hikasa and M. Kobayashi, Phys. Rev. D **36**, 724 (1987).
 [8] C. Boehm, A. Djouadi and Y. Mambrini, Phys. Rev. D **61**, 095006 (2000).
 [9] W. Beenakker *et al.*, Nucl. Phys. B **515**, 3 (1998).
 [10] J. Pumplin *et al.*, J. High Energy Phys. **0207**, 012 (2002); D. Stump *et al.*, *ibid.*, **0310**, 046 (2003).
 [11] LEPSUSYWG, ALEPH, DELPHI, L3 and OPAL Collaborations, note LEPSUSYWG/04-02.1 (<http://lepsusy.web.cern.ch/lepsusy/Welcome.html>).
 [12] T. Affolder *et al.* (CDF Collaboration), Phys. Rev. Lett. **84**, 5704 (2000).
 [13] V.M. Abazov *et al.* (D0 Collaboration), Phys. Rev. Lett. **93**, 011801 (2004).
 [14] V.M. Abazov *et al.* (D0 Collaboration), Phys. Lett. B **640**, 230 (2006).
 [15] V.M. Abazov *et al.* (D0 Collaboration), Nucl. Instrum. and Methods A **565**, 463 (2006).
 [16] T. Andeen *et al.*, “Adjustments to the D0 Experiment’s Measured Luminosity for Tevatron Run IIa,” FERMILAB-TM-2365, in preparation.
 [17] G.C. Blazey *et al.*, “Run II Jet Physics: Proceedings of the Run II QCD and Weak Boson Physics Workshop,” arXiv: hep-ex/0005012.
 [18] R. Brun and F. Carminati, CERN Program Library Long Writeup W5013, 1993 (unpublished).
 [19] M.L. Mangano *et al.*, J. High Energy Phys. **0307**, 001 (2003).
 [20] T. Sjöstrand *et al.*, Comput. Phys. Commun. **135**, 238 (2001).
 [21] H.L. Lai *et al.* Eur. Phys. J. C **12**, 375 (2000).
 [22] J. Campbell and R.K. Ellis, Phys. Rev. D **60**, 113006 (1999).
 [23] B. Clément, Ph.D. thesis, Université Louis Pasteur, Strasbourg, N° d’ordre IPHC 06-004, N° d’ordre ULP 5086, FERMILAB-THESIS-2006-06 (2006).
 [24] T. Junk, Nucl. Instrum. and Methods A **434**, 435 (1999); A. Read, in “First Workshop on Confidence Limits,” CERN Report No. CERN-2000-005, 2000.
 [25] A. Heister *et al.* (ALEPH Collaboration), Phys. Lett. B **537**, 5 (2002).